

Measurement of the cross section for direct photon production in association with a heavy quark in $p\bar{p}$ collisions at $\sqrt{s} = 1.96$ TeV

Ray Culbertson¹, Costas Vellidis², and Tingjun Yang³

FNAL

Abstract

We present the measurement of the cross section for direct photon production in association with a heavy quark (b or c) jet in $p\bar{p}$ collisions at $\sqrt{s} = 1.96$ TeV. The data sample used corresponds to an integrated luminosity of 9.1 fb^{-1} collected with the CDF II detector. Measurements are performed as a function of the photon transverse energy, covering photon transverse energy $30 < E_T^\gamma < 300$ GeV, photon rapidities $|y^\gamma| < 1.0$, jet transverse energy $E_T^{jet} > 20$ GeV, and jet rapidities $|y^{jet}| < 1.5$.

Contents

1	Introduction	2
2	Data and Monte Carlo samples	2
3	Event selection	3
4	Cross section measurement	3
4.1	Photon fraction	4
4.2	b/c /Light-jet fractions	6
4.3	Unfolding factors	10
5	Theoretical predictions	13
6	Cross section results	14
7	Summary	16

¹rlc@fnal.gov

²vellidis@fnal.gov

³tjyang@fnal.gov

A MC M_{SecVtx} shapes	16
B Reproduce CDF 340 pb^{-1} results	19
C Reproduce D0 1.0 fb^{-1} results	19
D Mock data challenge	21

1 Introduction

Photons produced in association with heavy quarks Q (c or b) in the final state of hadron-hadron interactions provide valuable information about the parton distributions of the initial state hadrons. Such events are produced primarily through the QCD Compton-like scattering process $gQ \rightarrow \gamma Q$ (Fig.1(a)), which dominates at low photon transverse energy, but also through quark-antiquark annihilation $q\bar{q} \rightarrow \gamma g \rightarrow \gamma Q\bar{Q}$ (Fig.1(b)), which dominates at high photon transverse energy [1]. Consequently, $\gamma + Q + X$ production is sensitive to the b , c , and g densities within the colliding hadrons, and can provide constraints on parton distribution functions (PDFs) that have large uncertainties. Moreover, many searches for new physics will benefit from a more precise knowledge of the heavy quark and gluon content of the proton.

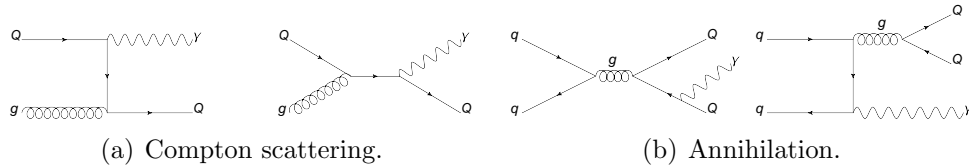


Figure 1: Feynman diagrams for the Compton scattering (a) and annihilation (b) subprocesses.

In this note, we describe a measurement of $\gamma + b/c + X$ production cross sections. We present the cross sections both as a function of photon E_T and for all photons with an E_T exceeding 30 GeV.

2 Data and Monte Carlo samples

The main dataset used in this analysis is the inclusive photon dataset, covering the periods 0-38 of data taking, i.e. the full CDF Run II dataset. The integrated luminosity is 9.1 fb^{-1} . Three jet datasets with different E_T thresholds are used to model the shape of photon ID likelihood of fake photon background and to validate the shape of secondary vertex mass template of light-flavor quarks.

Monte Carlo samples are used to construct the templates (photon ID likelihood, secondary vertex mass of tagged jets) to derive the photon and b/c -jet fractions. They

are also used to unfold the measurement back to the hadron level. All the MC samples used are Gen6 PYTHIA Tune A with realistic simulation. The generation has been done with different cuts on \hat{p}_T to guarantee enough statistics along the p_T range considered in this measurement. Inclusive photon MC samples are used to estimate the photon fraction and to unfold the measurement back to the hadron level. Di-jet MC samples are used to estimate the fake photon and b/c -jet fractions

3 Event selection

The data are required to have passed one of the following trigger paths: PHOTON_25_ISO, ULTRA_PHOTON_50 or SUPER_PHOTON_70 EM or JET. The SUPER_PHOTON_70 trigger only applies a loose E_T cut and a loose Had/EM cut, which prevents a potential inefficiency arising at high E_T where the EM energy becomes saturated causing the HAD/EM to be miscalculated. Since we explore the photon E_T spectrum above 30 GeV, the trigger efficiency is taken as 100% [2].

All events are first required to be marked “good” for photons and btags using the goodrun list. To select events consistent with a beam-beam interaction, the event must have a class 12 vertex and the primary z-vertex of the event has to be in the range $|Z_{event}| < 60$ cm. The events are then required to have a central photon ($|\eta^\gamma| < 1$) of $30 < E_T^\gamma < 300$ GeV, and a jet of level-7 corrected E_T^{jet} exceeding 20 GeV within $|\eta^{jet}| < 1.5$. The photon must pass the loose photon ID cuts and the artificial neural network (ANN) photon ID cut: $ANN > 0.75^4$ [3]. Reference [4] uses $Z \rightarrow ee$ events in data and MC to derive an energy scale correction, based on comparing the MC and data Z mass peaks. This energy scale correction is applied to this analysis. Jets are reconstructed with algorithm JetClu cone 0.4. The selected jet must have a positive SECVTX tag and lie outside a cone of $\Delta R = 0.4$ surrounding the photon candidate. The cross sections are measured in the 8 E_T^γ bins: [30,35], [35,40], [40,50], [50,70], [70,90], [90,120], [120,170], and [170,300] (all in GeV).

4 Cross section measurement

The cross section is calculated as follows:

$$\frac{d\sigma}{dE_T^\gamma} = \frac{N_{evt} \times f_\gamma \times f_{b/c}}{UF_{b/c} \times L \times \Delta E_T^\gamma}, \quad (1)$$

where N_{evt} is the number of selected data events in each photon E_T bin, f_γ is the photon fraction, $f_{b/c}$ is the b/c -jet fraction after subtracting fake photons, $UF_{b/c} = \varepsilon_{trig}\varepsilon_{reco}\varepsilon_\gamma\varepsilon_{b/c}$ is the unfolding factor that takes into account the trigger, reconstruction, photon ID, heavy-flavor tagging efficiencies and unfolds the measurement back to the parton level, L is the data luminosity, and ΔE_T^γ is the width of the E_T^γ range.

⁴This cut was chosen to be the same as in the Higgs to $\gamma\gamma$ analysis [9] since we use the $Z \rightarrow ee$ based corrections to photon ID efficiency developed in that analysis.

There are two main background sources: π^0 and η decays to two or more photons that fake a single photon shower and light-flavor jets (u , d , or s) that fake heavy-flavor jets. To get the photon fraction, we fit the data ANN output distribution using the signal and background templates. To get the b -jet fraction, we fit the data secondary vertex invariant mass distribution using the light/ c / b -jet templates.

4.1 Photon fraction

The photon candidates are selected using the ANN photon ID. The shapes of the ANN output distributions are different for the prompt photons and fake photons from π^0 and η decays as shown in Fig.2, which allows us to get the prompt photon fraction by fitting the data ANN distributions to the two templates. The signal distribution

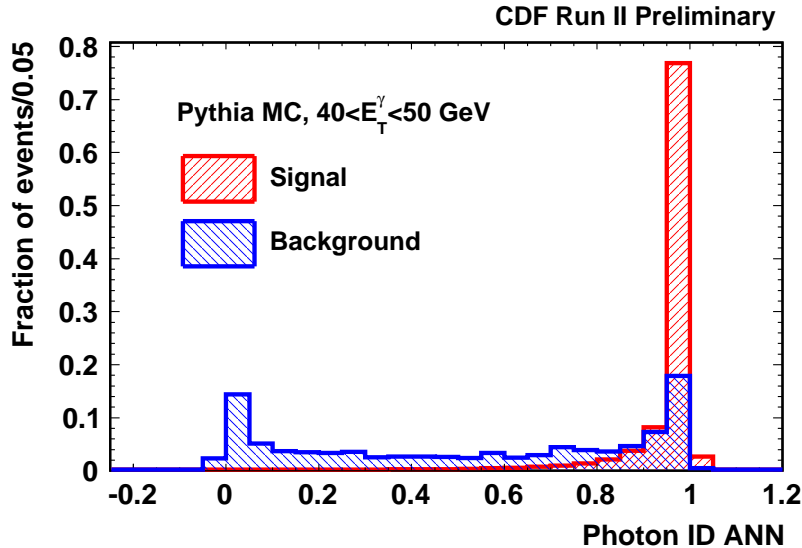


Figure 2: ANN output distributions for signal (prompt photons) and background (π^0 and η decays).

is constructed from inclusive photon MC. The background distribution is constructed from di-jet MC where contributions from initial state radiation (ISR) and final state radiation (FSR) are removed since these are prompt photons from hard scattering and should be considered as signals. Events should have at least one photon candidate that passes the loose photon ID cuts [3]. In each E_T^γ bin, we reweigh the MC events to have the same N_{vertex} distribution as observed in data to take into account effects dependent on luminosity.

The photon fraction is estimated by fitting the photon ID ANN distribution in the data using TMinuit to the signal and background MC ANN templates in each E_T^γ bin.

The χ^2 in TMinuit is defined as:

$$\chi^2 = \sum_{i=1}^N [N_{data} - xN_{sig} - (1-x)N_{bg}]^2 / [\varepsilon_{data}^2 + x^2\varepsilon_{sig}^2 + (1-x)^2\varepsilon_{bg}^2], \quad (2)$$

where N is the number of bins in the photon ID ANN histograms and x is the signal fraction. The signal and background templates are normalized to the total number of data events. Fig. 3 shows the results of the fits for $30 < E_T^\gamma < 300$ GeV. Fig. 4 shows the photon fraction as a function of E_T^γ . To calculate the photon fraction, we integrate the best fit signal and background templates for ANN>0.75 and divide signal by signal + background. Statistical errors of data and templates and correlations between templates are reflected in the statistical errors on the fitted fractions.

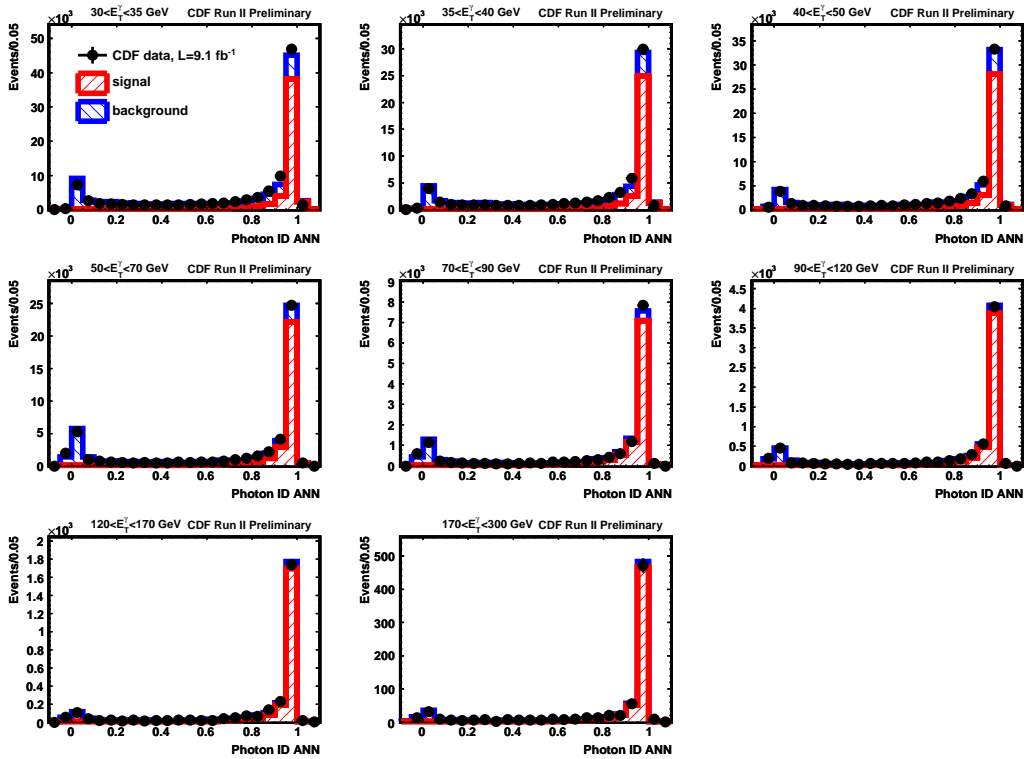


Figure 3: Fits to the ANN distributions in bins of E_T for $30 < E_T^\gamma < 300$ GeV.

The following systematic effects are evaluated.

Photon energy scale We consider $\pm 1.5\%$ systematics in the photon energy scale according to the studies in [5]. This uncertainty takes into account both geometrical and energy dependence differences between data and MC. We vary the E_T^γ by $\pm 1.5\%$ in MC. This will make events migrate between E_T^γ bins and change the ANN template shapes.

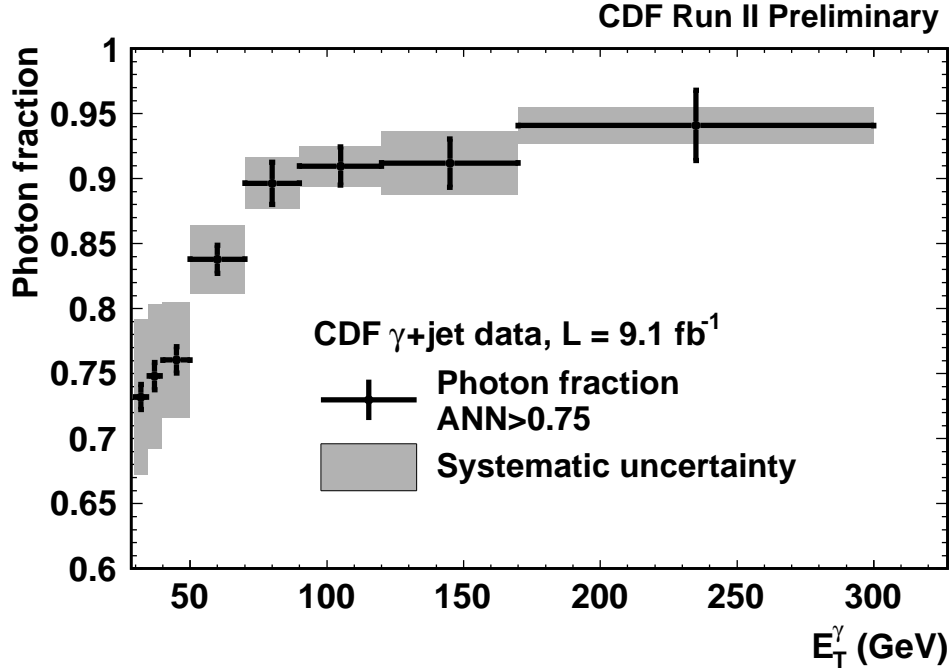


Figure 4: Photon fraction for ANN > 0.75 as a function of E_T^γ . The error bars represent the statistical errors and the gray bands represent the systematic errors.

ANN variables Some ANN input variables are less than well modeled in the MC. We vary 3 ANN input variables (EIso4, CES_CEM, and HadEm)⁵ by $\pm 50\%$ based on data and simulation comparisons to study how sensitive the result is to the mismodeling of the ANN variables. This turns out to be a small systematic effect.

ANN binning By default we use 40 bins, from -0.5 to 1.5, for the ANN histograms. We use two different binnings to test sensitivity to shapes: 80 bins and 3 bins. For the 3-bin case, the ANN range is divided into 3 regions: ANN < 0.25, 0.25 < ANN < 0.75, and ANN > 0.75. Using different binnings has a rather large effect (approximately 7%) at low photon E_T .

Figure 5 shows the total systematic uncertainty and relative contributions on the photon fraction as a function of photon E_T . The dominant systematic effect at low E_T^γ is ANN binning and the dominant effect at high E_T^γ is the ANN input variable EIso4.

4.2 b/c /Light-jet fractions

We use the secondary vertex (SECVTX) b-tagger to select heavy-flavor jets and we use the invariant mass of the tracks associated with the secondary vertex (M_{SecVtx}) to discriminate between b , c and light quark jets. Fig. 6 shows the secondary vertex

⁵The meanings of these variables can be found in [3]

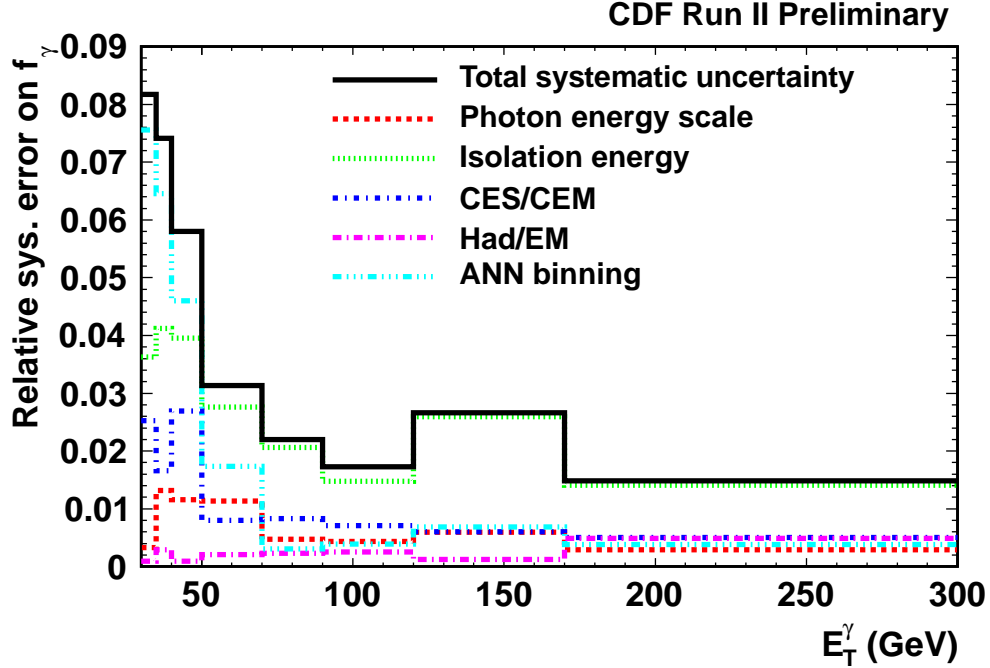


Figure 5: Total systematic uncertainty and relative contributions on the photon fraction as a function of photon E_T .

mass distributions for each type. We reweigh MC events to have the same N_{vertex} and tagged jet E_T distributions as observed in photon data in each E_T^γ . The b -jet template has a long tail due to the B meson decays. The c -jet template has a sharp edge at around 1.8 GeV due to the D meson decays. The light-jet template tends to have lower mass. However, at high E_T the light-jet template has a longer tail and looks more similar to the c -jet template, which makes it harder to discriminate between these two components.

We subtract the fake photon background contribution from the data secondary vertex invariant mass distribution before we fit the data. The shape of fake photon background component is modeled using inclusive jet data. We require there are at least two jets in the event. One jet (photon-like jet) must be in the central calorimeter ($|\eta^{j1}| < 1$) and pass the cut $\text{HadEm} < 0.125$ so that it mimics a central photon. The other jet must have a positive SECVTX tag (tagged jet) and lie outside a cone of $\Delta R = 0.4$ surrounding the photon-like jet. The tagged jet must pass the same cuts as applied to the photon data: $|\eta^{j2}| < 1.5$ and $E_T^{j2} > 20$ GeV. The events are reweighed so that the tagged jet E_T distribution matches that observed in the inclusive photon dataset (cph1). The M_{SecVtx} distribution of the tagged jets is then normalized to the predicted number of fake photons obtained by the ANN fit described in the previous section. The error of this background prediction is propagated to the fit described below.

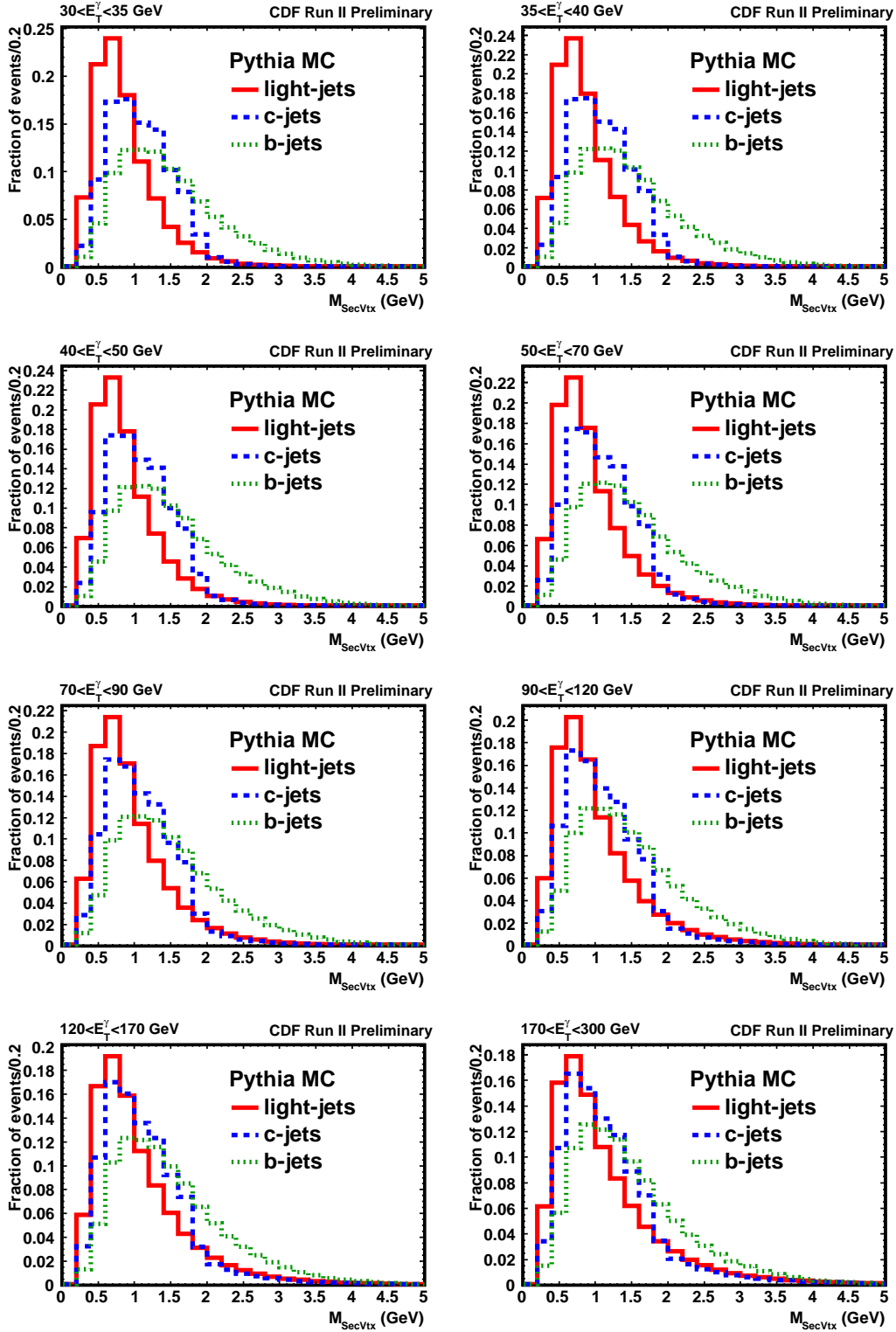


Figure 6: Secondary vertex mass templates for b , c , and light quark jets, obtained from PYTHIA MC. MC distributions are reweighted according to the tagged jet E_T observed in data for various E_T^γ ranges.

We fit the secondary vertex mass distribution in data to three templates (b/c /light-jet) after subtracting the fake photon background using TMinuit. Fig. 7 shows the results of the fits in the 8 bins of photon E_T for $30 < E_T^\gamma < 300$ GeV. We justify and correct MC template shapes based on electron jets and negative tags. The details are discussed in Appendix A. The MC templates are reweighed according to the N_{vertex} and tagged jet E_T distributions observed in the inclusive photon data in each photon E_T bin.

Fig. 8 shows the results of the fits for b fraction, c fraction, and light fraction after subtracting the contributions from fake photons, shown as a function of photon E_T .

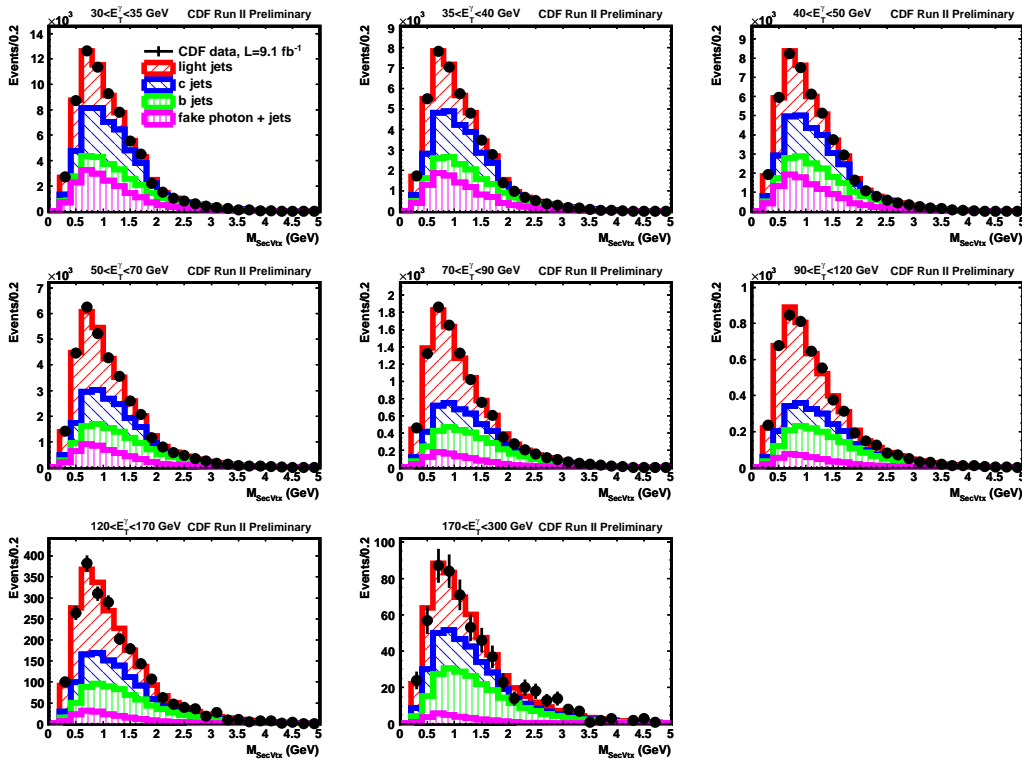


Figure 7: Fits to secondary vertex mass distributions in data in each photon E_T bin. The outcome of the fit is shown as the red histogram, and the components are overlaid in shaded areas.

We evaluate the following systematic effects on the b/c /light-jet fractions.

Jet energy scale We vary the jet energy scale by $\pm 1\sigma$ using the standard routines. This only affects the event acceptance. It does not change the template shapes so the effect is small.

Template shapes It has been estimated that tracking efficiency is 3% worse in data [7]. A 3% inefficiency leads to a 3% downward shift in template mass. To

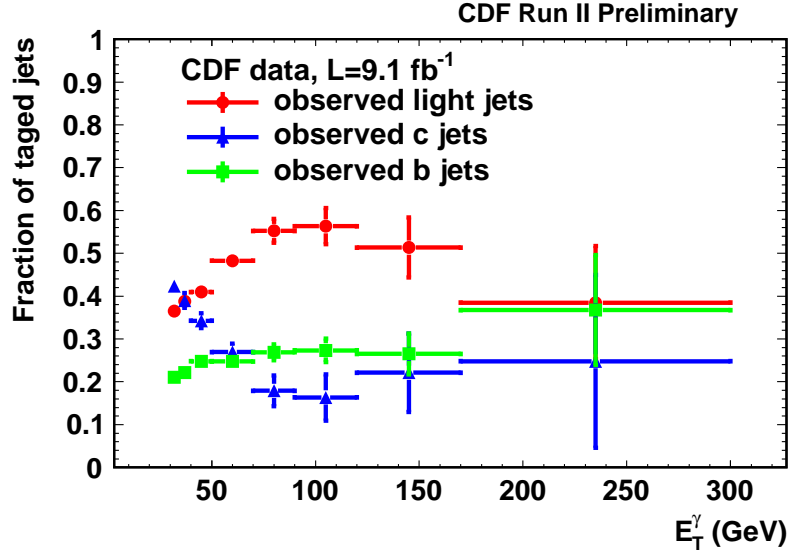


Figure 8: Results of jet composition fits for b fraction, c fraction, and light fraction after subtracting the contributions from fake photons, shown as a function of photon E_T . The error bars represent the statistical errors.

study this effect, we scale the templates by $\pm 3\%$ [8] and then refit data. This gives the largest systematic error on the b/c /light-jet fractions (approximately 20%). However, this systematic error is quite conservative especially at high E_T^{jet} considering the studies we did on the template shapes (See Appendix A).

Difference between single-quark jet and two-quark jet It is possible for one or two heavy quarks to lie inside the same jet. The contribution from two-quark jets is important especially at high photon E_T where the dominant process is annihilation followed by gluon splitting. For the tagged b -jet, the two- b jet fraction is 7% at $E_T^{jet} = 20$ GeV and increases to 30% at $E_T^{jet} = 200$ GeV. There is a difference in the secondary vertex mass between single-quark jets and two-quark jets. To evaluate this systematic effect, we reduce the contributions from two- c or two- b jets by 50% or increase their contributions by a factor of two and then refit data using the new templates. The resulting systematic error is negligible at low photon E_T but increases to approximately 20% at high photon E_T .

Figure 9 shows the b/c /light-jet fractions in the tagged jets as a function of photon E_T and the systematic errors on these fractions.

4.3 Unfolding factors

We use the PYTHIA inclusive photon MC sample to unfold the detector effects. The unfolding factors correct for acceptance and smearing effects, and also account for the

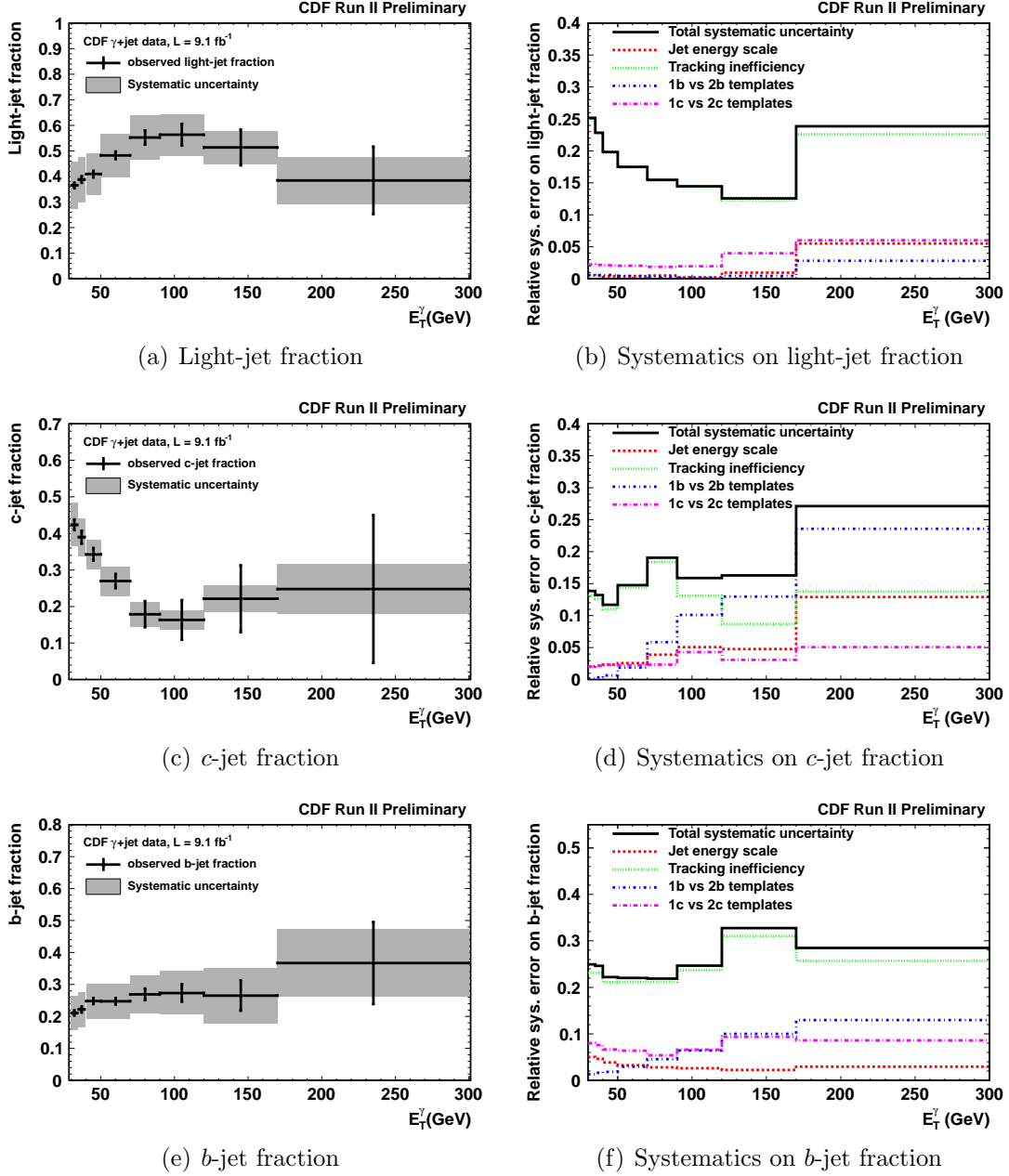


Figure 9: Observed light-jet, b -jet, and c -jet fractions as a function of photon E_T and the systematic errors on these fractions.

efficiencies of the photon selection and heavy-flavor jet tagging. The numerator is calculated using events passing the following cuts:

- A photon candidate in the central calorimeter passing the loose photon ID cuts and ANN photon ID cut: $\text{ANN} > 0.75$ with reconstructed $30 < E_T^\gamma < 300$ GeV.
- A positively tagged jet in the region $|\eta^{jet}| < 1.5$ with reconstructed $E_T^{jet} > 20$

GeV. There is either a b quark or a c quark in a cone of 0.4 around the jet.

- ΔR between the photon and jet is larger than 0.4.

The denominator is calculated using events passing the following cuts:

- A generated photon in the region $|y^\gamma| < 1$ with $30 < p_T^\gamma < 300$ GeV and $E_{iso} < 2$ GeV in the cone of 0.4 around the photon.
- A generated b or c quark in the region $|y^{b/c}| < 1.5$ with $p_T^{b/c} > 20$ GeV.
- ΔR between the photon and b or c quark is larger than 0.4.

Reference [9] uses $Z \rightarrow ee$ events in data and MC to derive a correction to the ANN photon ID cut efficiency reported by the MC. We apply this photon ID efficiency correction to this analysis. We also apply the recommended scale factor 0.95 ± 0.05 [10] to correct the b tagging efficiency. The effects of underlying events are also corrected for in the unfolding factors.

Figure 10 shows the unfolding factors for $\gamma + b + X$ and $\gamma + c + X$ measurements as a function of photon E_T .

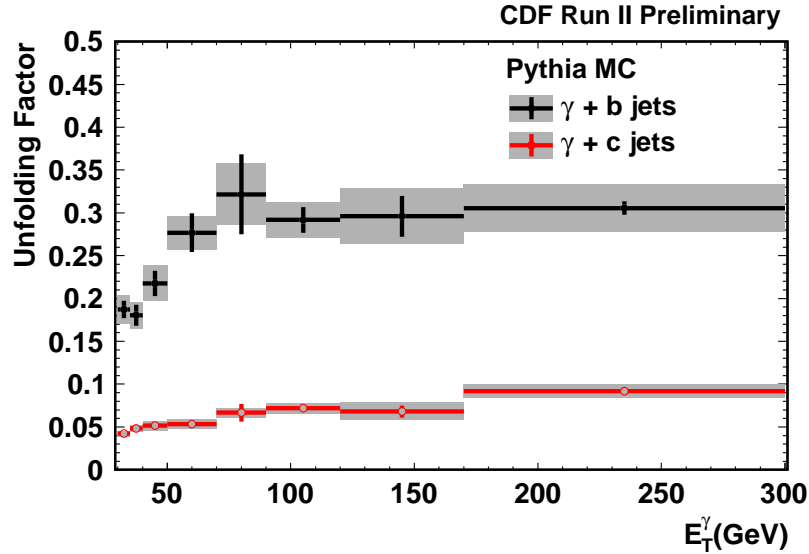


Figure 10: Unfolding factors as a function of photon E_T . The error bars represent the MC statistical errors and the gray bands represent the systematic errors.

We evaluate the following systematic effects in the same way as described in the previous sections: photon energy scale, photon ID (ANN variables and binning), jet energy scale. We assign a 5% systematic error on the b -tagging efficiency [10] and a 3% error from PDF uncertainties [2]. Fig. 11 shows the systematic errors on the unfolding factors. The total systematic errors are approximately 10% for both $\gamma + b + X$ and $\gamma + c + X$ unfolding factors.

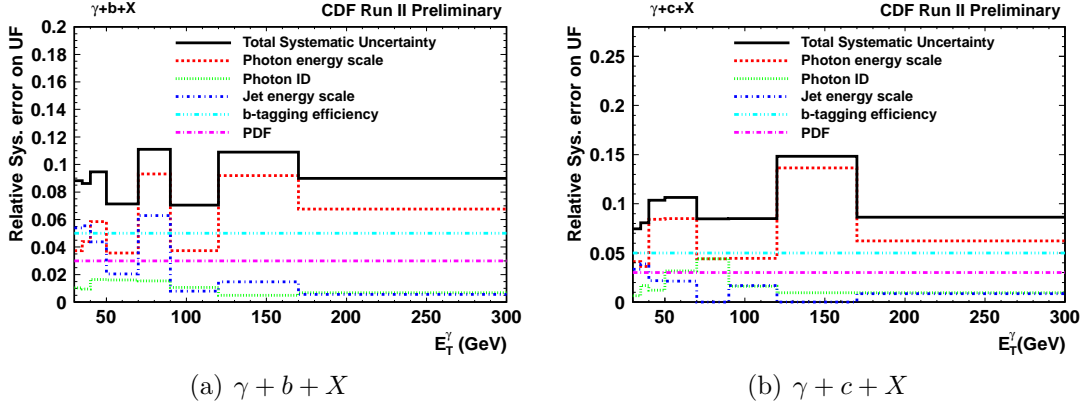


Figure 11: Systematic errors on the unfolding factors.

5 Theoretical predictions

We compare our measurements to two theoretical predictions: next-to-leading order calculation (NLO) and PYTHIA. Stavreva and Owens performed a next-to-leading calculation of the inclusive cross section for a photon and a heavy quark (charm or bottom) in [1]. Pointlike photon subprocesses through $\mathcal{O}(\alpha\alpha_s^2)$ and fragmentation subprocesses through $\mathcal{O}(\alpha_s^3)$ are included. The calculation is performed using a phase space slicing technique so that the effects of experimental cuts can be included. CTEQ6.6M PDFs were used in the calculation. The QCD Compton-like scattering subprocess $gQ \rightarrow \gamma Q$ (Fig.1(a)) dominates at low photon transverse energy, while the quark-antiquark annihilation subprocess $q\bar{q} \rightarrow \gamma g \rightarrow \gamma Q\bar{Q}$ (Fig.1(b)) overtakes the Compton contribution and starts dominating the cross section at $E_T^\gamma \sim 70$ GeV. However, as stated in [1], there is no Born term which involves a $q\bar{q}$ initial state and, therefore, the contributions from the annihilation subprocess start in $\mathcal{O}(\alpha\alpha_s^2)$. As such, the typical compensation between LO and NLO contributions for this subprocess is missing, and the annihilation subprocess can be thought of a leading order. This indicates this NLO calculation may not be sufficient to describe data at high E_T^γ since it is missing loop and higher order corrections. The authors also calculated the $\gamma + c + X$ cross section using two models that study the possibility for an intrinsic charm component of the nucleon: BHPS model, which is a light-cone model, and the sea-like model in which the charm distribution follows the shape of the light flavor sea quarks.

For comparison, we also calculate the cross section for a photon and a heavy quark using PYTHIA 6.226. We set MSEL = 10, which includes 5 prompt photon production subprocesses:

$$14 \quad q_i\bar{q}_i \rightarrow g\gamma$$

$$18 \quad f_i\bar{f}_i \rightarrow \gamma\gamma$$

$$29 \quad q_i g \rightarrow q_i\gamma$$

114 $gg \rightarrow \gamma\gamma$

115 $gg \rightarrow g\gamma$

Subprocess 29 gives the contribution of Compton scattering subprocess if the heavy quark is radiatively generated from the gluon's PDF. Subprocess 14 followed by gluon splitting gives the contribution of annihilation subprocess. The rate of gluon splitting to heavy quarks may be underestimated in PYTHIA [13]. We also calculated the cross sections using modified PYTHIA parameters to enhance the rate of gluon splitting to heavy quarks: $\text{mstj}(42)=4$ and $\text{mstj}(44)=3$.

Both calculations apply the following kinematic cuts:

- $|y^\gamma| < 1$ with $30 < p_T^\gamma < 300$ GeV and $E_T^{\text{iso}} < 2$ GeV in the cone of 0.4 around the photon.
- $|y^{b/c}| < 1.5$ with $p_T^{b/c} > 20$ GeV.
- ΔR between the photon and the leading b or c quark is larger than 0.4.

6 Cross section results

The cross sections are calculated using Eq. 1. Tables 1 and 2 show the measured cross sections for $p\bar{p} \rightarrow \gamma + b + X$ and $p\bar{p} \rightarrow \gamma + c + X$. Figs. 12 and 13 shows the cross sections as a function of photon E_T . Fig. 14 shows the systematic errors on the $\gamma + b + X$ and $\gamma + c + X$ cross sections as a function of photon E_T . The systematic error on luminosity is taken as 6%.

The total cross section $\sigma(p\bar{p} \rightarrow \gamma + b + X; 30 < E_T^\gamma < 300 \text{ GeV}, p_T^b > 20 \text{ GeV})$ is measured to be $19.7 \pm 0.7(\text{stat}) \pm 5.0(\text{syst})$ pb. The corresponding NLO prediction is $27.3_{-1.5}^{+2.3}$ pb. The PYTHIA prediction is 17.0 pb.

The total cross section $\sigma(p\bar{p} \rightarrow \gamma + c + X; 30 < E_T^\gamma < 300 \text{ GeV}, p_T^c > 20 \text{ GeV})$ is measured to be $132.2 \pm 4.6(\text{stat}) \pm 19.2(\text{syst})$ pb. The corresponding NLO prediction is $152.6_{-9.6}^{+12.2}$ pb. The PYTHIA prediction is 101.3 pb.

The NLO calculations agree reasonably well with data at low E_T^γ . At high E_T^γ data are higher than the NLO predictions. The discrepancy may be caused by several effects:

- Missing loop and higher order corrections in the NLO calculations.
- Mismodeling of gluon splitting rate to heavy quarks.
- Possible contributions from intrinsic heavy quarks.

More theoretical studies are needed to understand these effects.

E_T^γ (GeV)	N_{data}	f_γ	f_b	UF_b	$\frac{d\sigma}{dE_T^\gamma}$ (pb/GeV)	NLO (pb/GeV)	PYTHIA (pb/GeV)
30-35	70227	0.732	0.211	0.187	$1.27 \pm 0.09 \pm 0.37$	2.23	1.26
35-40	43953	0.748	0.222	0.180	$(8.85 \pm 0.73 \pm 2.48) \times 10^{-1}$	1.24	7.52×10^{-1}
40-50	47346	0.761	0.248	0.217	$(4.49 \pm 0.36 \pm 1.18) \times 10^{-1}$	5.66×10^{-1}	3.69×10^{-1}
50-70	34192	0.838	0.248	0.277	$(1.40 \pm 0.13 \pm 0.34) \times 10^{-1}$	1.58×10^{-1}	1.11×10^{-1}
70-90	10470	0.896	0.269	0.322	$(4.29 \pm 0.69 \pm 1.09) \times 10^{-2}$	3.76×10^{-2}	2.90×10^{-2}
90-120	5290	0.910	0.273	0.292	$(1.65 \pm 0.19 \pm 0.44) \times 10^{-2}$	1.03×10^{-2}	8.90×10^{-3}
120-170	2264	0.912	0.265	0.296	$(4.05 \pm 0.81 \pm 1.44) \times 10^{-3}$	2.18×10^{-3}	2.19×10^{-3}
170-300	594	0.941	0.367	0.306	$(5.66 \pm 2.00 \pm 1.73) \times 10^{-4}$	2.08×10^{-4}	2.56×10^{-4}

Table 1: Data yields, photon fractions, b -jet fractions, unfolding factors, measured cross sections, NLO calculations, and PYTHIA calculations for $p\bar{p} \rightarrow \gamma + b + X$. Statistical uncertainties take into account both the data and MC statistics.

E_T^γ (GeV)	N_{data}	f_γ	f_c	UF_c	$\frac{d\sigma}{dE_T^\gamma}$ (pb/GeV)	NLO (pb/GeV)	PYTHIA (pb/GeV)
30-35	70227	0.732	0.424	0.042	$(1.13 \pm 0.06 \pm 0.19) \times 10$	1.36×10	8.73
35-40	43953	0.748	0.390	0.048	$5.80 \pm 0.40 \pm 0.93$	7.05	4.67
40-50	47346	0.761	0.343	0.052	$2.61 \pm 0.20 \pm 0.44$	3.02	2.06
50-70	34192	0.838	0.270	0.053	$(7.93 \pm 0.83 \pm 1.55) \times 10^{-1}$	7.39×10^{-1}	5.25×10^{-1}
70-90	10470	0.896	0.179	0.067	$(1.38 \pm 0.35 \pm 0.30) \times 10^{-1}$	1.44×10^{-1}	1.08×10^{-1}
90-120	5290	0.910	0.163	0.072	$(3.98 \pm 1.34 \pm 0.77) \times 10^{-2}$	3.17×10^{-2}	2.60×10^{-2}
120-170	2264	0.912	0.221	0.068	$(1.47 \pm 0.63 \pm 0.30) \times 10^{-2}$	5.09×10^{-3}	5.02×10^{-3}
170-300	594	0.941	0.248	0.092	$(1.27 \pm 1.04 \pm 0.38) \times 10^{-3}$	3.72×10^{-4}	4.84×10^{-4}

Table 2: Data yields, photon fractions, c -jet fractions, unfolding factors, measured cross sections, NLO calculations, and PYTHIA calculations for $p\bar{p} \rightarrow \gamma + c + X$. Statistical uncertainties take into account both the data and MC statistics.

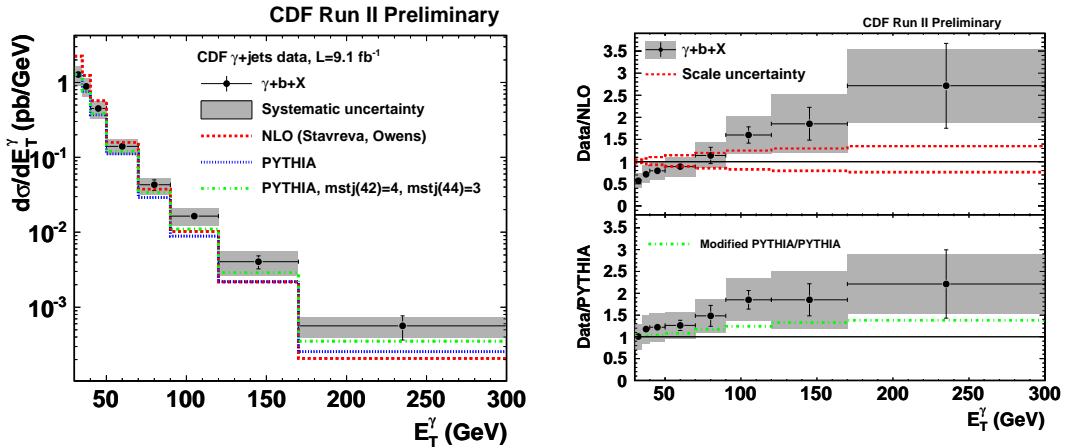


Figure 12: The measured $\gamma + b + X$ cross section compared with two theoretical predictions

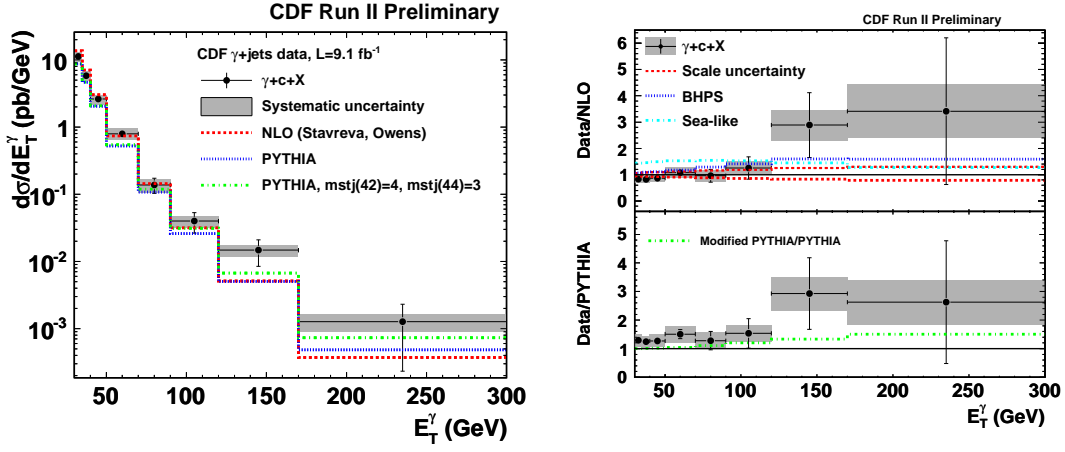
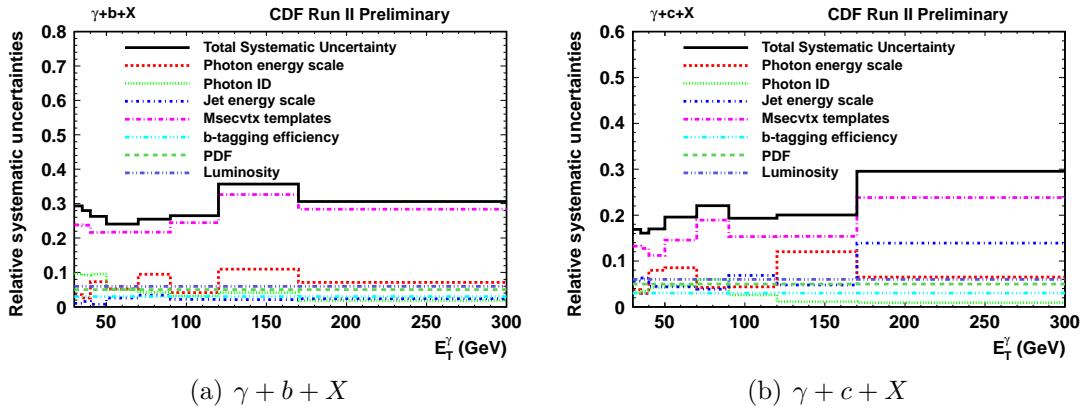


Figure 13: The measured $\gamma + c + X$ cross section compared with two theoretical predictions



(a) $\gamma + b + X$

(b) $\gamma + c + X$

Figure 14: Systematic errors on the $\gamma + b + X$ and $\gamma + c + X$ cross sections as a function of photon E_T .

7 Summary

We have measured the cross sections for direct photon production in association with a b or c quark for photons with $\eta^\gamma < 1$, $E_T^\gamma > 30$ GeV and calorimeter isolation < 2 GeV and for b/c quarks with $\eta^{b/c} < 1.5$, $p_T^{b/c} > 20$ GeV and $\Delta R(\gamma, b/c) > 0.4$ using $9.1 fb^{-1}$ of data taken by the CDF II detector. Comparisons with two theoretical predictions are presented and discussed.

A MC M_{SecVtx} shapes

The M_{SecVtx} template shapes are very important for deriving the b -jet and c -jet fractions in data. We justify the MC M_{SecVtx} template shapes using various datasets.

We use **blpc** dataset (8 GeV electron calibration sample) and employ the “electron method” for deriving b-tagging scale factors [6] to justify the heavy-flavor jet templates. The MC samples used are **bt0sla** and **bt0sld** (di-jet samples filtered for electrons). The events must contain two jets. One of these jets, the “electron jet”, must contain an electron with $E_T > 9$ GeV within ΔR of 0.4 of the jet axis, and the isolation requirement for the electron is removed. This presence of electron enhances the heavy flavor content of the jets, due to the semileptonic decays of B or D mesons. Cuts are applied to remove photon conversions. Fig. 15 shows the M_{SecVtx} templates for the heavy-flavor enhanced data and MC samples. MC models the templates reasonably well.

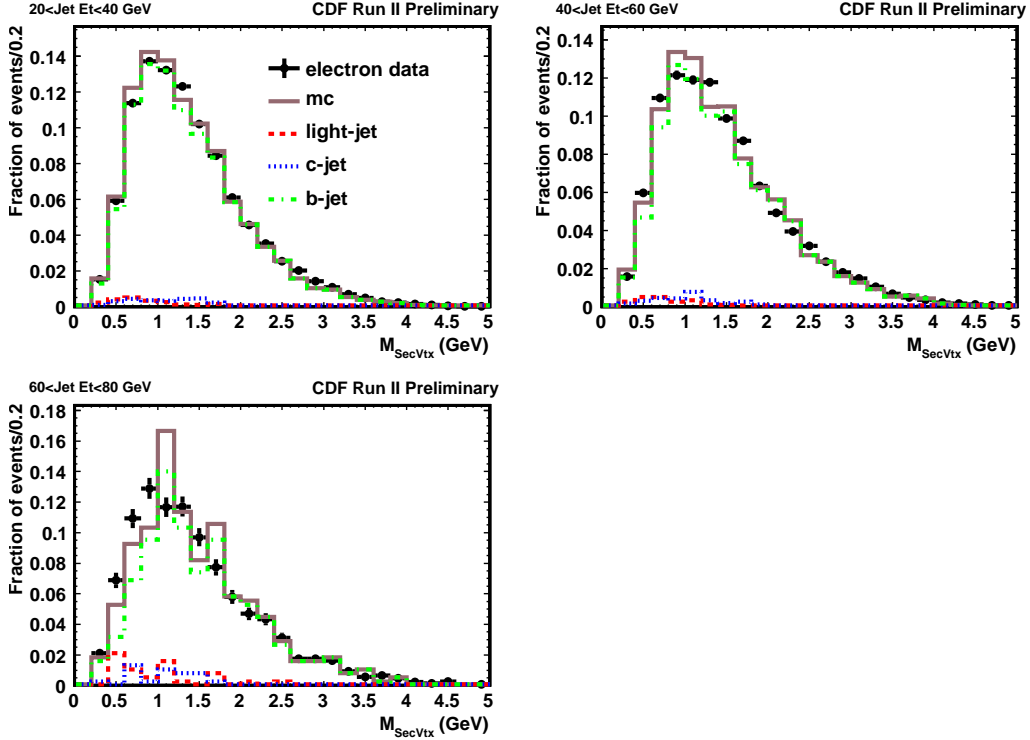


Figure 15: M_{SecVtx} templates for heavy-flavor enhanced data and MC samples.

We use the jets with negative SECVTX tags in the inclusive jet datasets to justify the light-flavor templates since the negatively tagged jets are predominantly light-flavor jets. Fig. 16 shows the M_{SecVtx} templates for the light-flavor enhanced data and MC samples.

Table 3 shows the mean values of M_{SecVtx} templates. The data/MC ratios are used to correct MC templates.

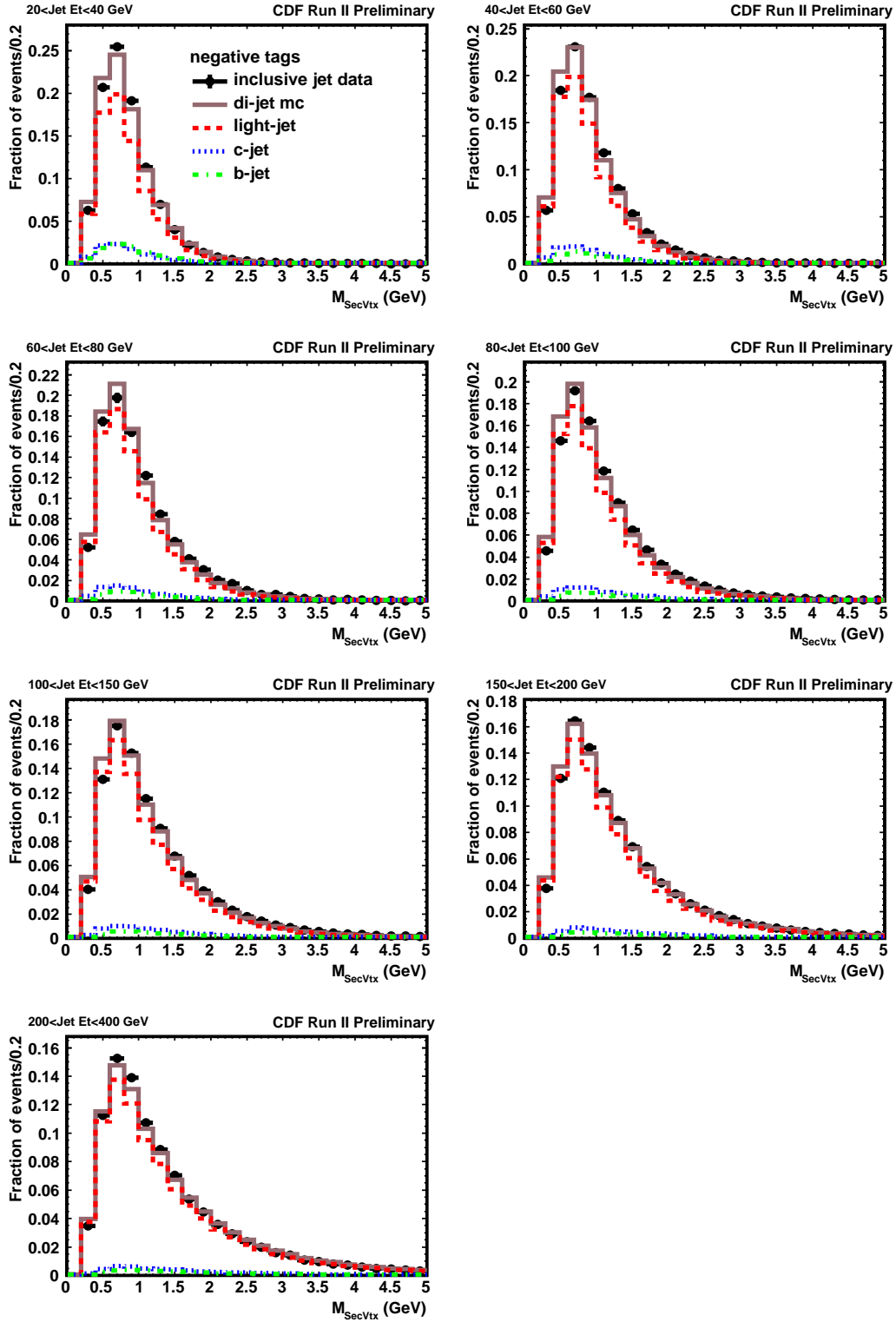


Figure 16: M_{SecVtx} templates for the negatively tagged jets in the inclusive jet data and di-jet MC samples.

E_T^{jet} ranges (GeV)	(20,40)	(40,60)	(60,80)	(80,100)	(100,150)	(150,200)	(200,400)
Heavy-flavor enhanced							
Data mean (GeV)	1.399	1.472	1.448				
MC mean (GeV)	1.361	1.455	1.468				
Data/MC	1.03	1.01	0.99				
Light-flavor enhanced							
Data mean (GeV)	0.880	0.958	1.046	1.125	1.225	1.308	1.399
MC mean (GeV)	0.869	0.918	0.995	1.071	1.175	1.289	1.414
Data/MC	1.01	1.04	1.05	1.05	1.04	1.01	0.98

Table 3: Mean values of M_{SecVtx} templates.

B Reproduce CDF 340 pb⁻¹ results

CDF published the measurement of $\gamma + b + X$ cross section in 2009 [11] based on two photon datasets: 208 pb⁻¹ photon+SVT trigger data (for $E_T^\gamma < 31$ GeV) and 340 pb⁻¹ inclusive photon data (for $E_T^\gamma > 31$ GeV). We have tried to reproduce that result using 9.1 fb⁻¹ inclusive photon data for $E_T^\gamma > 31$ GeV. Fig. 17 shows the comparison between the old results and the new results and they agree well. The new results have substantially smaller statistical errors but more conservative systematic errors. The old analysis used JetClu cone size 0.7 and required $\Delta R(\gamma, b) > 0.7$, while the new analysis uses JetClu cone size 0.4 and requires $\Delta R(\gamma, b) > 0.4$. However, the resulting difference seems rather small. We use the same binning as the old analysis for direct comparison. We also compare the NLO calculations done in 2006 and 2011. The latest calculation predicts higher cross section in the bin between 30 GeV and 35 GeV. This needs to be investigated.

C Reproduce D0 1.0 fb⁻¹ results

D0 published their measurements of $\gamma + b + X$ and $\gamma + c + X$ cross section in 2009 [12] using 1.0 fb⁻¹ of Run II data. Their measured $\gamma + b + X$ cross section agrees well with NLO prediction but the $\gamma + c + X$ cross section deviates from NLO prediction at high E_T^γ . They used different kinematic and isolation cuts than ours and we have tried to reproduce their results using the same cuts. The cuts D0 used are:

- $E_T^\gamma > 30$ GeV and $|\eta^\gamma| < 1$
- $E_h < 0.04E_\gamma$ for $\Delta R < 0.2$ and $E_h < 0.07E_\gamma$ for $\Delta R < 0.4$
- $p_T^{b/c} > 15$ GeV and $|\eta^{b/c}| < 0.8$

Figs. 18 and 20 show the results for $\gamma + b + X$ and $\gamma + c + X$ cross sections. The CDF results are consistent with D0's except the last bin in $\gamma + b + X$ spectrum. That bin shows

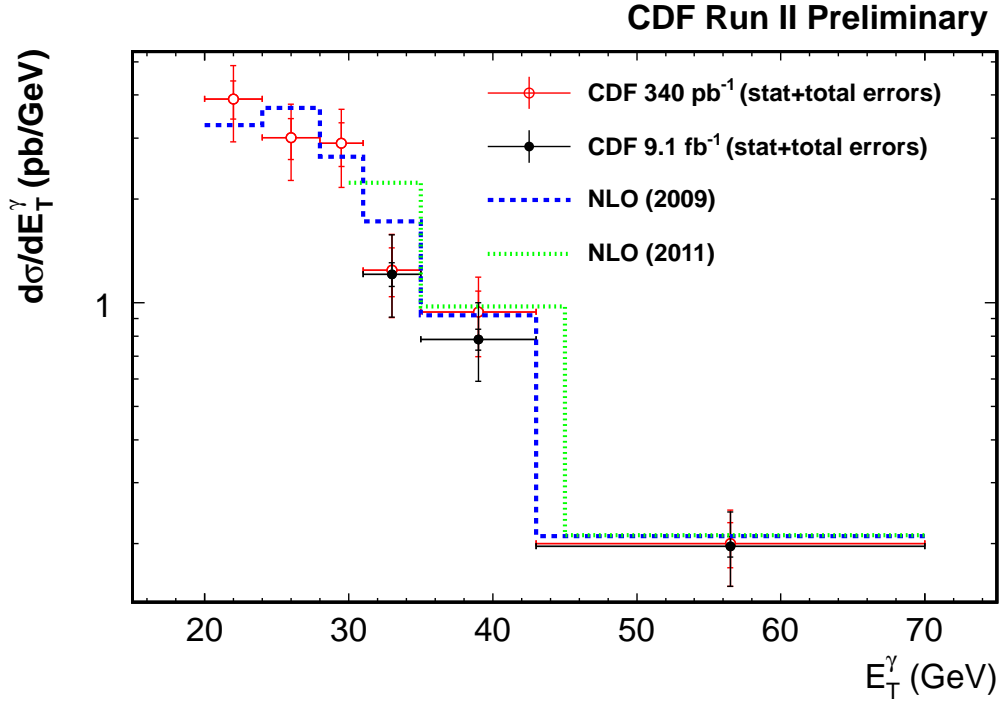
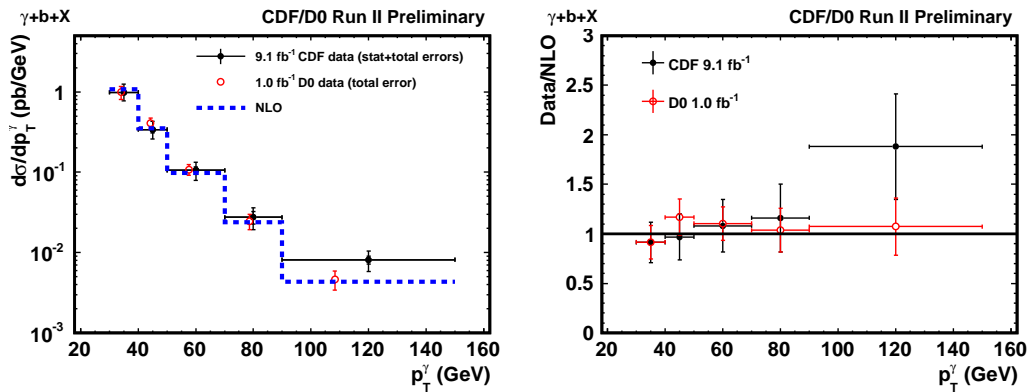


Figure 17: Comparison between the old analysis and the new analysis.

a 1.5σ difference, which is not significant. Fig. 20 shows ratios of $\gamma + c + X/\gamma + b + X$. We believe the ratio is a better measured and modeled quantity due to the cancellation of systematic errors. The CDF measured ratio agrees better with the NLO prediction than the D0 result does.

Figure 18: Reproducing D0's $\gamma + b + X$ cross section results.

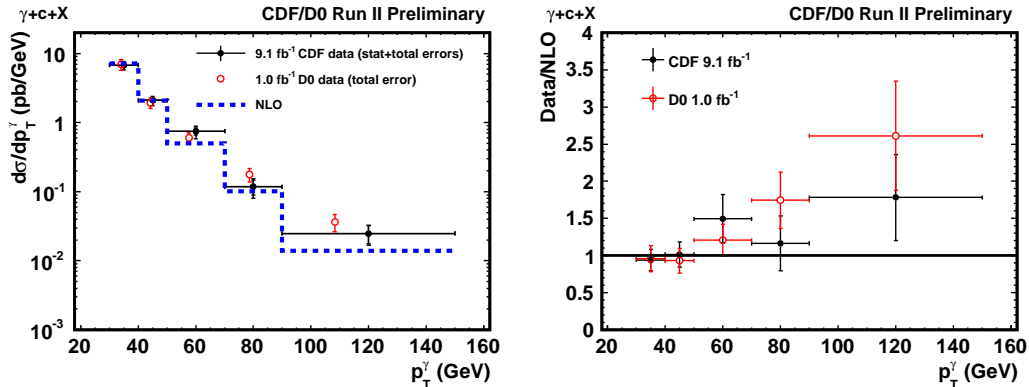


Figure 19: Reproducing D0's $\gamma + c + X$ cross section results.

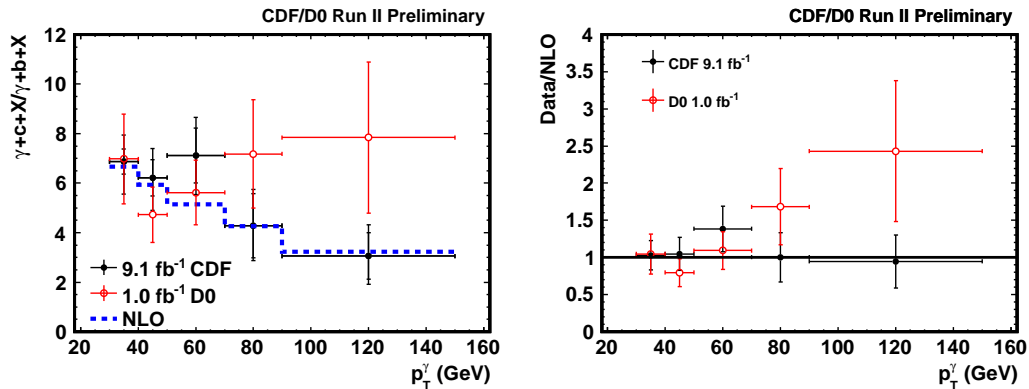


Figure 20: Ratio of $\gamma + c + X/\gamma + b + X$.

D Mock data challenge

We perform a mock data challenge using the inclusive photon MC. The inclusive photon MC samples are generated using PYTHIA. We treat the inclusive photon MC as data and try to derive the cross sections predicted by PYTHIA using the same techniques developed for the real data. This provides a test of the whole analysis chain. The fitted true photon fraction is consistent with being 1, which is expected. Figs.21 and 22 shows the fitted light/ c / b -jet fractions. Fig.23 shows the measured cross sections, which agree with PYTHIA predictions well.

References

- [1] T. P. Stavreva and J. F. Owens, Phys. Rev. D **79**, 054017 (2009) [arXiv:0901.3791 [hep-ph]].

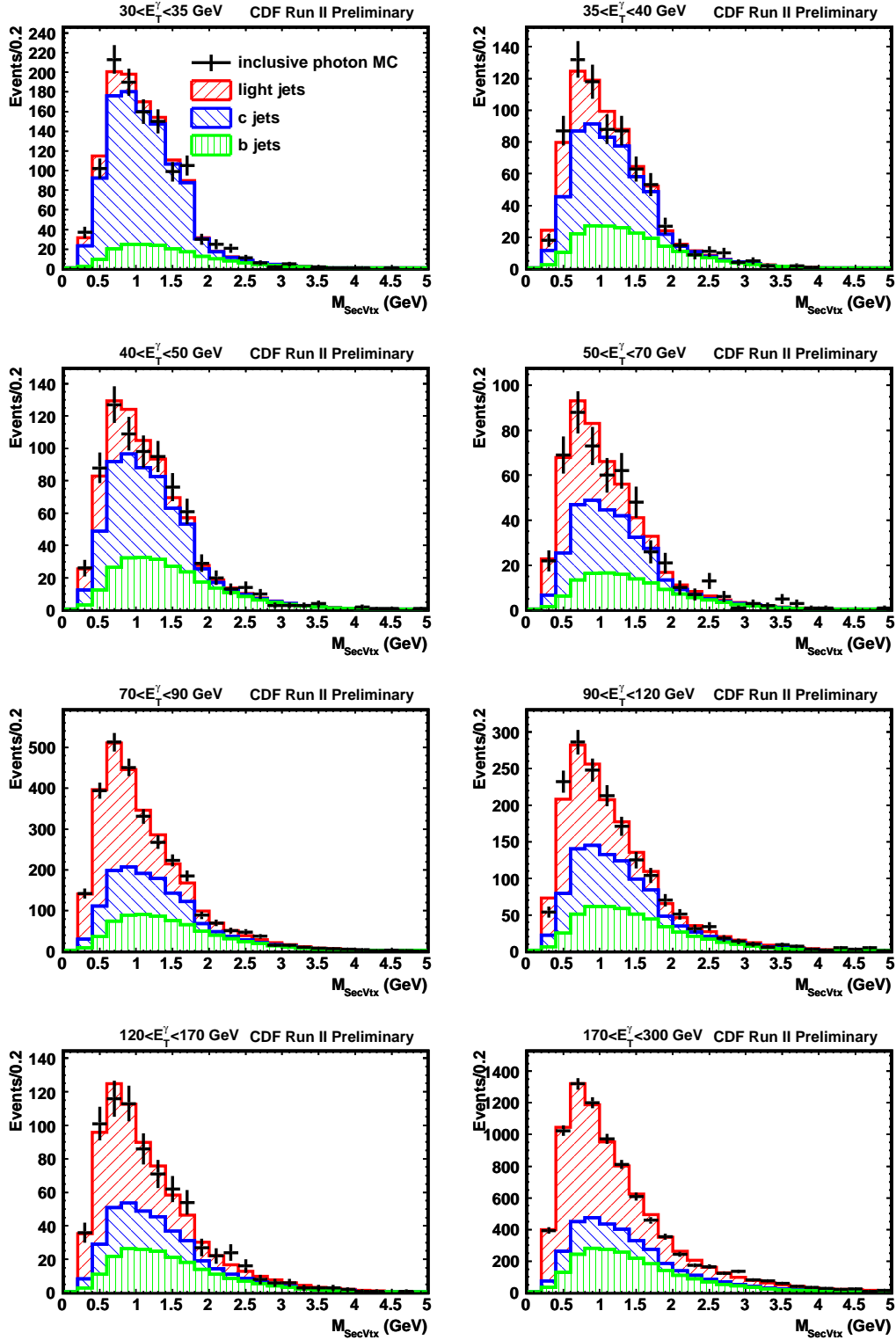


Figure 21: Fits to secondary vertex mass distributions in inclusive photon MC in each photon E_T bin. The outcome of the fit is shown as the red histogram, and the components are overlaid in shaded areas.

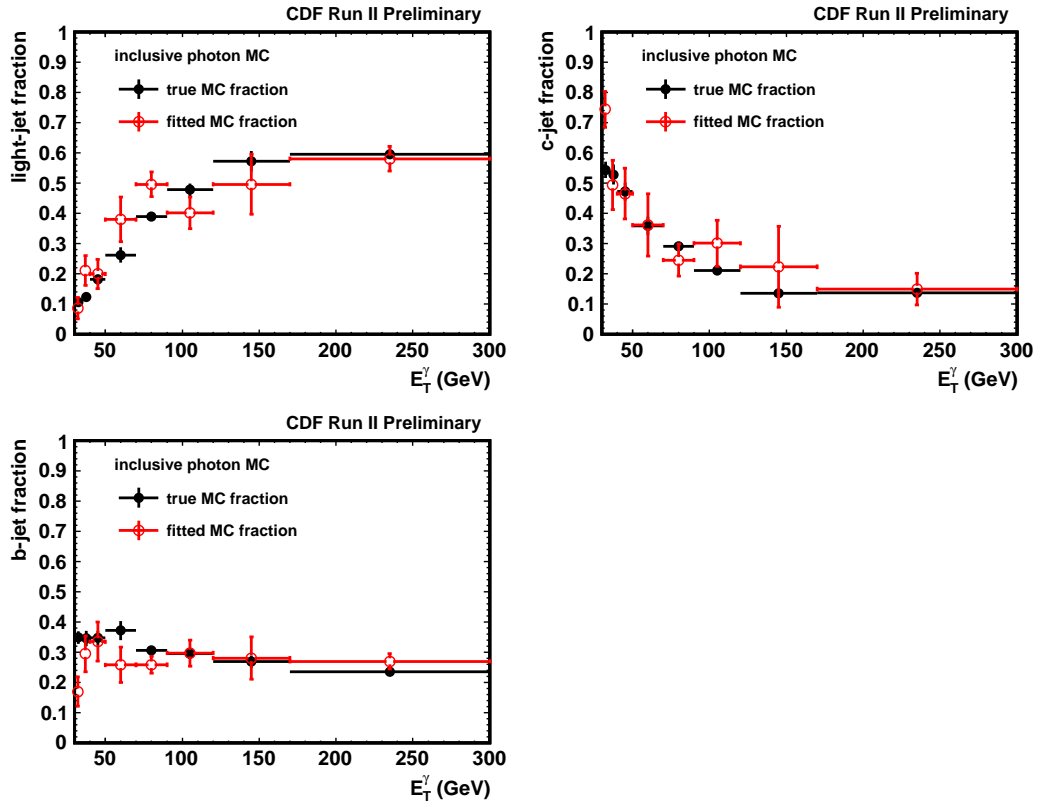


Figure 22: Results of jet composition fits for light fraction, c fraction, and b fraction shown as a function of photon E_T . The error bars represent the statistical errors.

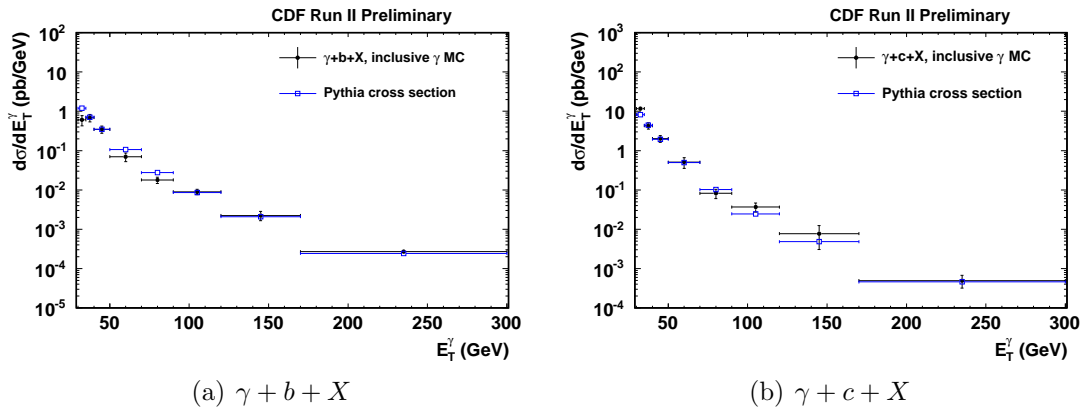


Figure 23: Reproducing PYTHIA cross sections, statistical errors only

- [2] R. Culbertson *et al*, "Measurement of the Inclusive and Isolated Prompt Photon Cross Section at CDF", [CDF Note 9590](#).
- [3] J. Ray *et al*, "Multivariate Photon ID for CDF", [CDF Note 10282](#).

- [4] R. Culbertson *et al.*, “Measurement of the central diphoton production cross section at CDF”, [CDF Note 10009](#).
- [5] S. Yu *et al.*, “Studies of Electron and Photon Energy Scales”, [CDF Note 9591](#).
- [6] V. Giakoumopoulou and J. Freeman, “Summer 2010 SevVtx Scale Factors Calculated Using the Electron Method through Period 28”, [CDF Note 10178](#).
- [7] S. Sabik and P. Savard, “Track reconstruction efficiency in jets”, [CDF Note 6894](#).
- [8] R. McNulty and T. Shears, “Photon + b jet production at CDF”, [CDF Note 8329](#).
- [9] K. Bland *et al.*, “Search for a SM and fermiophobic Higgs Boson in the Diphoton Final State”, [CDF Note 10724](#).
- [10] <http://www-cdf.fnal.gov/internal/physics/top/RunIIBtag/bTag.html>.
- [11] T. Aaltonen *et al.* [CDF Collaboration], *Phys. Rev. D* **81**, 052006 (2010) [[arXiv:0912.3453 \[hep-ex\]](#)].
- [12] V. M. Abazov *et al.* [D0 Collaboration], *Phys. Rev. Lett.* **102**, 192002 (2009) [[arXiv:0901.0739 \[hep-ex\]](#)].
- [13] A. Ballestrero, P. Bambade, S. Bravo, M. Cacciari, M. Costa, W. deBoer, G. Dissertori and U. Flammeyer *et al.*, In *Geneva 1999/2000, Reports of the working groups on precision calculation for LEP2 physics* 137-218 [[hep-ph/0006259](#)].